A mouse model of hereditary folate malabsorption: deletion of the *PCFT* gene leads to systemic folate deficiency

Konstantin V. Salojin,[1] Robert M. Cabrera,[2] Weimei Sun,[1] Wei Chun Chang,[1] Colin Lin,[1] Lindsay Duncan,[1] Ken A. Platt,[1] Robert Read,[1] Peter Vogel,[1] Qingyun Liu,[1] Richard H. Finnell,[2,3] and Tamas Oravecz[1]

[1]Lexicon Pharmaceuticals, Inc, The Woodlands, TX; [2]Texas A&M Institute for Genomic Medicine, Houston, TX; and [3]Institute of Biosciences and Technology, TX A&M Health Science Center, Houston, TX

The human proton coupled folate transporter (PCFT) is involved in low pH-dependent intestinal folate transport. In this report, we describe a new murine model of the hereditary folate malabsorption syndrome that we developed through targeted disruption of the first 3 coding exons of the murine homolog of the *PCFT* gene. By 4 weeks of age, *PCFT*-deficient (*PCFT*$^{-/-}$) mice developed severe macrocytic normochromic anemia and pancytopenia. Immature erythroblasts accumulated in the bone marrow and spleen of *PCFT*$^{-/-}$ mice and failed to differentiate further, showing an increased rate of apoptosis in intermediate erythroblasts and reduced release of reticulocytes. In response to the inefficient hematologic development, the serum of the *PCFT*$^{-/-}$ animals contained elevated concentrations of erythropoietin, soluble transferrin receptor (sCD71), and thrombopoietin. In vivo folate uptake experiments demonstrated a systemic folate deficiency caused by disruption of PCFT-mediated intestinal folate uptake, thus confirming in vivo a critical and nonredundant role of the PCFT protein in intestinal folate transport and erythropoiesis. The *PCFT*-deficient mouse serves as a model for the hereditary folate malabsorption syndrome and is the most accurate animal model of folate deficiency anemia described to date that closely captures the spectrum of pathology typical of this disease. (*Blood*. 2011;117(18):4895-4904)

Introduction

Folate is an essential cosubstrate of many biochemical reactions, such as the de novo synthesis of purines and pyrimidines, methionine, and deoxythymidylate monophosphate.[1,2] Mammals cannot synthesize folate; therefore, inadequate dietary supply or folate malabsorption results in defective DNA synthesis. One of the first manifestations of a folate deficiency is in the rapidly proliferating cells of the hematopoietic system, leading to pancytopenia and anemia of the megaloblastic type. Patients with megaloblastic anemia demonstrate ineffective erythropoiesis by harboring large immature red blood cell (RBC) precursors that fail to survive to the postmitotic, terminal stages, undergoing premature apoptosis.[2]

Three mammalian folate transporter systems have been described to date in a variety of tissues: (1) the bidirectional reduced folate carrier 1 (RFC1), also known as SLC19A1,[3,4] (2) the glycosyl-phosphatidylinositol-anchored folate receptors (FOLR1, FOLR2, and FOLR4) and one secreted receptor in humans without a mouse homolog (FOLR3),[5] and (3) the human proton coupled folate transporter (PCFT).[6-8] The RFC1 transporter is expressed ubiquitously, including the brush-border membrane of epithelial cells in the small intestine.[9] Although RFC1 is necessary for folate transport in erythroid cells, its involvement in intestinal folate uptake has not been confirmed.[6] Inactivation of RFC1 in mice by homologous recombination led to either embryonic lethality or defective erythropoiesis in pups born to mothers who were supplemented with 1 mg daily subcutaneous doses of folic acid.[10,11] Because this transporter functions at a neutral pH optimum whereas the majority of intestinal folate transport occurs in an acidic luminal milieu, RFC1 is an unlikely candidate for an intestinal folate transporter.[7] The role of FOLR1 in folate absorption and transport has also been demonstrated, where a 60% to 70% reduction was observed in plasma folate of *FOLR1*$^{-/-}$ mice fed low folate and normal chow.[12] FOLR1 also regulates folate homeostasis via endocytotic mechanisms during embryonic development, and mice rendered null for this receptor display severe morphogenetic abnormalities and die in utero unless provided supraphysiologic concentrations of either folinic acid or 5-methyltetrahydrofolate.[5,13]

The PCFT transporter is highly expressed in tissues involved in folate and heme transport, including the duodenum and liver.[6,14] Initially, PCFT was identified as a low-affinity, pH-independent heme transporter[14] and then later described to function as a low pH-dependent folate transporter in intestinal cells.[6] The latter role of the transporter was confirmed by the identification of loss-of-function mutations in the human *PCFT* gene in persons diagnosed with hereditary folate malabsorption syndrome.[6] Studies have also indicated that PCFT facilitates folate transport during folate receptor-mediated endocytosis, where FOLR1 binds folate, and its export into the cytosol is driven by PCFT activity as the vesicle undergoes endocytosis and becomes acidified.[15] In this report, we describe a new murine model of hereditary folate malabsorption syndrome and folate deficiency anemia, which we developed through targeted deletion of the *PCFT* gene, and confirm in vivo a critical and nonredundant role of the PCFT transporter in folate metabolism and erythropoiesis.

Submitted April 12, 2010; accepted February 2, 2011. Prepublished online as *Blood* First Edition paper, February 23, 2011; DOI 10.1182/blood-2010-04-279653.

The publication costs of this article were defrayed in part by page charge payment. Therefore, and solely to indicate this fact, this article is hereby marked "advertisement" in accordance with 18 USC section 1734.

An Inside *Blood* analysis of this article appears at the front of this issue.

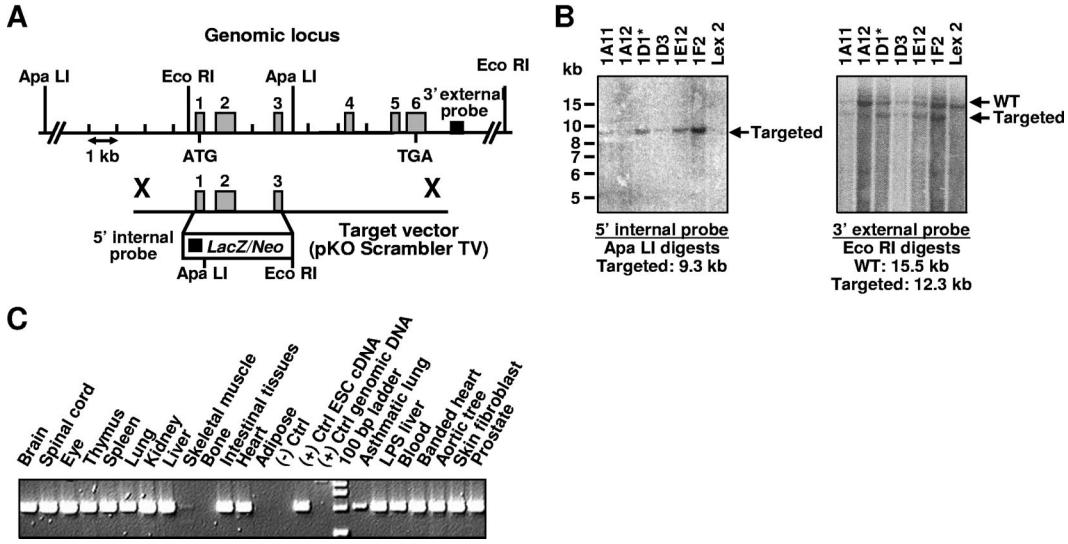

Figure 1. Targeted disruption and expression analysis of the *PCFT* gene. (A) Targeting strategy is shown, including relevant restriction sites used for confirmation of Southern hybridization analysis. Homologous recombination between the targeting vector and the *PCFT* gene replaced exons 1 to 3 with the selection cassette. The 5′ internal and 3′ external probes used for Southern hybridization analysis were designed inside and outside the target vector arms of homology, respectively. (B) Southern hybridization demonstrating proper targeting events in ESC clones. Clone 1D1 was selected for blastocyst injection; Lex2 indicates untransfected ESC DNA. (C) Expression of the *PCFT* gene was detected in ESCs and in all adult tissues by reverse-transcribed PCR, except bone and adipose.

Methods

Generation of *PCFT* mutant mice

The PCFT targeting vector was derived using long-range polymerase chain reaction (PCR) to generate the 5′ and 3′ arms of homology using 129/SvEv^{Brd} embryonic stem cell (ESC) Lex-1 DNA as a template. The 2388-bp 5′ arm was generated using primers PCFT-3 [5′-GGATCCG-GATGGGCTGAGCAGAGGGCAACGA-3′] and PCFT-2 [5′-GGCCGC-TATGGCCTGCGCAAACACGGAGGGGCTAGCAC-3′] and cloned using the TOPO cloning kit (Invitrogen). The 5722-bp 3′ arm was generated using primers PCFT-4 [5′-GGCCAGCGAGGCCGGATCAGTTTG-TATCTGGTCCCTCG-3′] and PCFT-6 [5′-CTCGAGCATGGCCTT-GCTCTGTAACTACCTG-3′] and cloned using the TOPO cloning kit. The 5′ arm was excised from the holding plasmid using *Bam*HI and SfiI. The 3′ arm was excised from the holding plasmid using SfiI and *Xho*I. The arms were ligated to a SfiI prepared selection cassette containing a β-galactosidase-neomycin fusion marker (B-Geo) along with a PGK promoter-driven puromycin resistance marker and inserted into a *Bam*HI/*Xho*I cut pKO Scrambler vector (Stratagene) to complete the PCFT targeting vector. The NotI linearized targeting vector was electroporated into 129/SvEv^{Brd} (Lex-1) ESCs. G418/FIAU-resistant ESC clones were isolated, and correctly targeted clones were identified and confirmed by Southern analysis using a 291-bp 5′ selection cassette probe (8/9), generated by PCR using primers Ires-8 [5′-AGGAAGCAGTTCCTCTGGAA-3′] and Ires-9 [5′-CACATGTAAAGCATGTGCACC-3′] and a 441-bp 3′ external probe (20/21), amplified by PCR using primers PCFT-20 [5′-GGCAACCTCAC-CTTACTCAAGC-3′] and PCFT-21 [5′-GGAGGCCACCATCGAGAA-3′]. Southern analysis using probe 8/9 detected a 9.3-kb mutant band in ApaL1 digested genomic DNA, whereas probe 20/21 detected a 15.5-kb wild-type (WT) band and 12.3-kb mutant band in *Eco*RI digested genomic DNA. Six targeted ESC clones were identified and microinjected into C57BL/6 (albino) blastocysts to generate chimeric animals, which were bred to C57BL/6 (albino) females. The resulting heterozygous (*PCFT*$^{+/-}$) offspring were interbred to produce homozygous *PCFT*$^{-/-}$ mice. Determination of the genotype of mice at the *PCFT* locus was performed by screening DNA from tail biopsy samples using quantitative PCR for the *Neo* cassette. This strategy enabled discrimination of zero, one, or 2 gene disruptions representing WT, *PCFT*$^{+/-}$, and *PCFT*$^{-/-}$ mice, respectively.

All experiments were performed on mice of mixed genetic background (129/SvEvBrd and C57BL/6J) representing both sexes of littermate mutant and WT animals. Procedures involving animals were conducted in conformity with the Institutional Animal Care and Use Committee guidelines that are in compliance with the state and federal laws.

Complete blood cell count and flow cytometry (FACS) analysis

Peripheral blood was collected from the retro-orbital plexus of mice anesthetized with isofluorane, using heparinized microhematocrit capillary tubes. Complete blood cell count was obtained using an automatic hematology analyzer (Cell-Dyn 3500R, Abbott Diagnostics), according to the manufacturer's instructions. Reticulocytes and reticulated platelets (rtPLT) were quantitated on a FACScan flow cytometer (BD Biosciences Immunocytometry Systems) after staining whole blood samples with Retic-COUNT (Thiazole Orange) reagent (BD Biosciences), according to the manufacturer's instructions. Reticulocyte production index (RPI) in *PCFT*$^{-/-}$ mice was calculated by multiplying the percentage of reticulocytes in whole blood by the ratio of peripheral blood hematocrit (HCT) to the mean HCT in the WT group (% reticulocyte × [HCT/mean WT HCT]). The RPI was further adjusted for the longer life span of reticulocytes in mice with low HCT by dividing RPI values by the reticulocyte maturation index, which was arbitrarily set to 1 for blood samples with HCT values in the 41% to 50% range, and 1.5 for blood samples with HCT values in the 30% to 40% range.

For analysis of bone marrow (BM), cells were harvested by flushing femurs and tibia with 5 mL of Hanks balanced salt solution supplemented with 5% fetal bovine serum (fluorescence-activated cell sorter [FACS] buffer) using a 27-gauge needle. Single splenocyte suspensions were prepared by passage through a 70-μm cell strainer in the presence of FACS buffer. For FACS analysis, cells were washed 2 times in FACS buffer, incubated with 1 μg of monoclonal antibodies to CD16/CD32 molecules (Fc Block, BD Biosciences PharMingen) for 15 minutes at 4°C, and stained for 30 minutes at 4°C in the dark with fluorochrome-conjugated anti-Ter119 and CD71 monoclonal antibodies (all purchased from BD Biosciences PharMingen). The cells were washed twice in FACS buffer before analysis. Anucleated erythrocytes with low forward scatter were not included in the analysis.

Histology

Freshly isolated mouse tissues were fixed in buffered neutral 10% formalin. Paraffin-embedded tissue was sectioned at 4 to 6 μm, mounted, and stained with hematoxylin and eosin or Gomori iron stain by standard methods, or

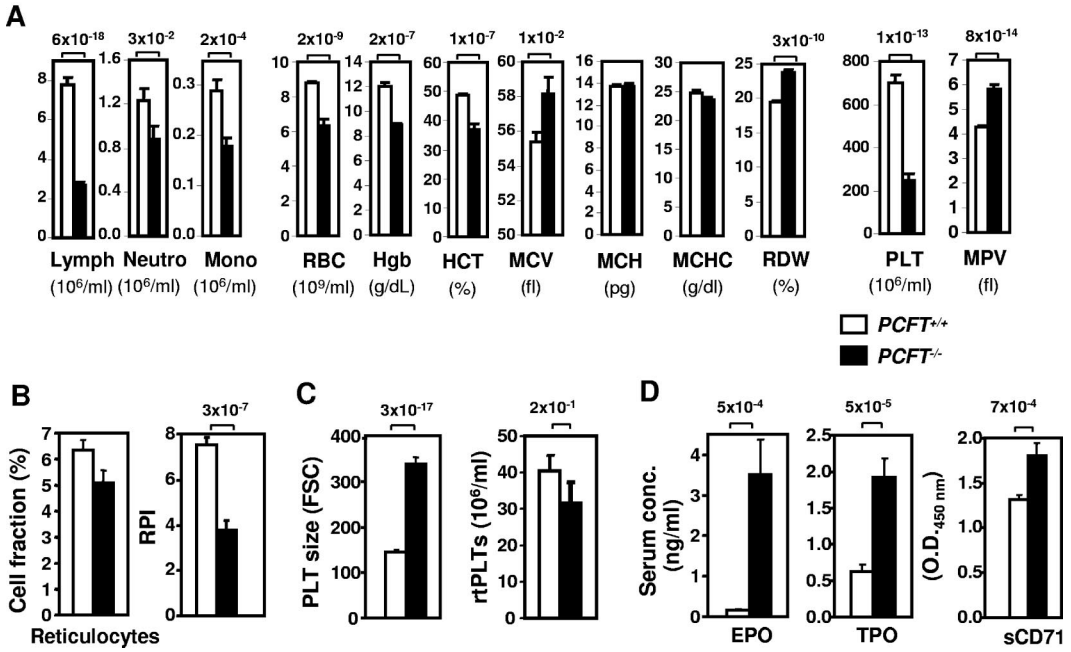

Figure 2. Hematologic profile of *PCFT*$^{-/-}$ mice is consistent with pancytopenia and ineffective erythropoiesis. (A) Hematologic parameters of mice with the indicated genotype at 4 to 6 weeks of age (n = 27-30 mice per cohort). Lymph indicates lymphocytes; Mono, monocytes; and Neutro, neutrophils. Additional RBCs (B) and PLT (C) parameters were assessed by FACS in the same cohorts of mice. (D) Serum concentrations of indicated soluble factors were measured in 15 to 46 mice of each genotype. All bar graph data are presented as mean ± SEM. Numbers above bars indicate *P* values.

modified von Kossa silver nitrate staining for Ca salts. Cytospin (Shandon Southern Products) preparations of BM cells and splenocytes were stained by the May-Grünwald-Giemsa standard technique. Sections and cytospin preparations were observed and photographed using the SPOT InSight 3.2.0 camera (Diagnostic Instruments Inc) attached to the Olympus BX51 microscope (Olympus), controlled by SPOT 4.0.9 software (Diagnostic Instruments Inc).

Enzyme-linked immunosorbent assays

Erythropoietin (EPO) and thrombopoietin serum levels were quantified using commercial enzyme-linked immunosorbent assay kits (R&D Systems). For measurement of soluble transferrin receptor (sCD71) concentration in mouse sera, Nunc Maxi-Sorp 96-well plates (VWR) were coated overnight at 4°C with 100 μL/well of a 5-μg/mL solution of rat antimouse CD71 IgG (Southern Biotechnology Associates). The plates were washed 3 times with phosphate buffered saline (PBS) containing 0.05% Tween-20 (PBS/Tween-20) and blocked with 200 μL/well of 10% fetal bovine serum in PBS for one hour at room temperature. After 5 washes in PBS/Tween-20, the plates were incubated with mouse serum (diluted 1:20 in PBS) for 2 hours at room temperature. Plate-bound sCD71 was detected by incubating the plates for one hour at room temperature with biotinylated rat antimouse CD71 IgG (2 μg/mL; BD Biosciences PharMingen), followed by streptavidin-conjugated horseradish peroxidase (30 minutes at room temperature; Southern Biotechnology Associates). Colorimetric detection was performed by adding 3,3′,5′,5-tetramethlybenzidine to the plates and reading absorbance at 450 nm wavelength.

Iron status, heme, folate, and homocysteine content measurements

Total serum iron (Fe^{2+} and Fe^{3+}) and tissue folate concentrations were measured using a colorimetric assay (QuantiChrom Iron Assay Kit, BioAssay Systems) and enzyme-linked immunosorbent assay (TECRA International), respectively, according to the protocols supplied by the manufacturers. For measurement of tissue folate, liver, kidney, and splenic tissues were weighed, homogenized, lysed by 3 cycles of freeze-thaw in folate enzyme-linked immunosorbent assay sample buffer, and briefly sonicated. Extracts were then centrifuged at 10 000*g* at 4°C, and the supernatant was retained.

Plasma folate was determined by modification of the inhibition of folate binding assay.[16] Briefly, bovine folate binding protein is immobilized onto glass slides and sample folates compete with horseradish peroxidase-labeled folic acid for binding to bovine folate binding protein. Standards of unlabeled folic acid (0.244-250 ng/mL) in PBS-0.1% Tween-20 (PBS-T, pH 7.3) were used to determine concentrations. Standards and plasma (10 μL) were diluted to 50 μL in PBS-TA (PBS-T with 1% weight/volume ascorbate, pH ~ 3.0) and placed in boiling water for 10 minutes. Samples were neutralized with 1 μL of 10% NaOH, checked for neutral pH on test strips, and spun for one minute at 14 000*g*. Supernatants were mixed 1:4 with horseradish peroxidase-labeled folic acid (Ortho-Clinical Diagnostics) and incubated with immobilized bovine folate binding protein for 2 hours. Slides were washed 5 times with PBS-T, signal amplification is performed with the biotin-labeled tyramide (PerkinElmer Life and Analytical Sciences), streptavidin-alkaline phosphatase conjugate (Invitrogen), and enzyme-labeled fluorescence alkaline phosphatase substrate (Invitrogen). Slides were imaged using an 8-bit UV photography workstation (Kodak). Fluorescent signal intensities were determined using ImageJ 1.43 (National Institutes of Health, Bethesda, MD), and foreground signals were fit with a sigmoid, regression curve using GraphPad Prism 4 Software.

Total homocysteine (tHcy) concentrations were determined in plasma and tissue homogenates using high-performance liquid chromatography according to the previously described procedure.[17,18] tHcy concentrations in tissue homogenates were further normalized to total protein content.

Analysis of in vivo folate uptake

Analysis of in vivo folate uptake was performed as previously described.[19] Briefly, a single intragastric dose of tritiated [3′,5′,7,9-^{3}H] folic acid (34.9 Ci/mmol; GE Healthcare) was given to mice by oral gavage (20 μCi/mouse). Control mice received a single oral dose of cold folic acid. Serum was collected by retrorbital bleed 0.5 and one hour after folate administration. Liver, kidney, proximal small intestine (duodenum and proximal jejunum), and spleen tissue were collected 16 hours after dosing, weighed, and homogenized in ice-cold 2 times radioimmunoprecipitation assay buffer (Thermo Fisher Scientific Inc) using a tissue homogenizer.

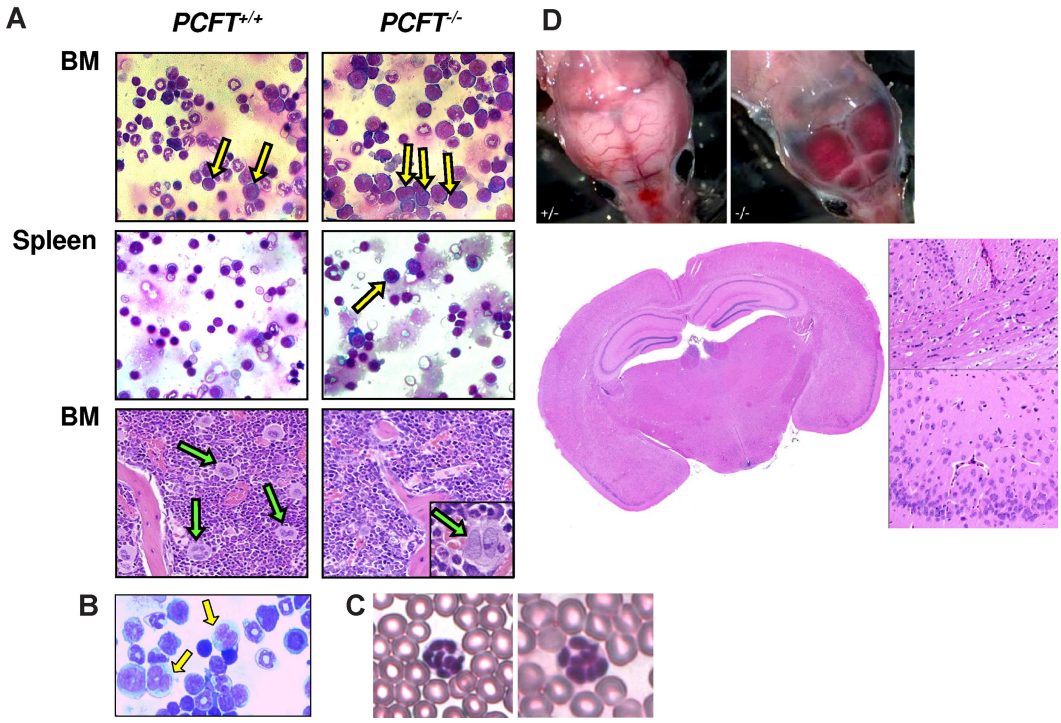

Figure 3. PCFT deficiency leads to impaired erythropoiesis and thrombopoiesis. (A) Representative May-Grünwald-Giemsa-stained cytocentrifuge preparations show accumulation of proerythroblasts and large basophilic erythroblasts (yellow arrows) in 4- to 6-week-old *PCFT*$^{-/-}$ mice. Periodic acid Schiff-stained BM sections (original magnification 10×/0.3 NA dry objective) contain reduced number of megakaryocytes (green arrows) in *PCFT*$^{-/-}$ mice than in WTs. (Inset) Megakaryocytes are less differentiated in the *PCFT*$^{-/-}$ BM, as evidenced by marked reduction in cytoplasmic volume and nuclear lobulation. (B) Abnormal neutrophil precursors (giant metamyelocytes, yellow arrows) in the BM of *PCFT*$^{-/-}$ mice (May-Grünwald-Giemsa staining of cytocentrifuge preparations). (C) Multilobed polymorphonuclear neutrophils in the *PCFT*$^{-/-}$ blood smears. (D) Representative picture of submeningeal hemorrhage in a *PCFT*$^{-/-}$ mouse (top panels) (original magnification 40×/0.75 NA dry objective). No evidence of deep intracerebral hemorrhage and calcification was found in *PCFT*$^{-/-}$ brain sections by hematoxylin and eosin (bottom panel) and von Kossa staining (not shown). The hematoxylin and eosin low power image (original magnification 2×/0.08 NA dry objective) corresponds to the location of the insets at the right (original magnification 20×/0.75 NA dry objective; sagittal fissure above corpus callosum and ventrolateral cortex, respectively).

Protein concentration in the tissue lysates was analyzed by the Bradford assay. Folate-associated radioactivity in serum and tissue lysates containing equal amounts of protein was measured by β-scintillation counting and normalized to the mouse weight.

Analysis of in vitro uptake of folate and zinc protoporphyrin

The full-length coding sequences of human and mouse *PCFT* were cloned into the expression vector pIRESpuro2 (Clontech). The plasmids were transfected into HEK293 cells with Lipofectamine 2000 (Invitrogen), and uptake of folate was measured 24 hours later as described previously.[6] Zinc protoporphyrin uptake assays were carried out in HEK293 cells transiently transfected with human *PCFT* essentially as described previously.[14]

Supplementation studies

PCFT$^{-/-}$ mice were given daily supplementation containing iron or folate. The volumes administered were 0.10 mL per 10 g of body weight. Hemin was dissolved with 10% ammonium hydroxide in 0.15M NaCl to prepare a stock solution of 100 mg/mL, then further diluted with sterile 0.15M NaCl, and injected subcutaneously into mice (1, 10, and 25 mg/kg). Vehicle-injected mice received an identical NH_4OH-containing solution lacking hemin. Ferrous sulfate ($FeSO_4$) was dissolved in sterile reverse osmosis purified water and given by gavage (1, 10, and 40 mg/kg). Folates 5-formyltetrahydrofolate (folinic acid) and 5-methyltetrahydrofolate (5-MTHF) were dissolved in distilled water and given by gavage or injected subcutaneously at 40 mg/kg dose. Folic acid was administered daily by subcutaneous injection at 0.1 mg/kg dose, or given by gavage (0.1 and 2 mg/kg body weight). All reagents were from Sigma-Aldrich, unless indicated otherwise.

Statistical analysis

The normality of results was evaluated by the Kolmogorov-Smirnov test. Statistical significance of group differences between WT and *PCFT*$^{-/-}$ mice was analyzed using the 2-sample Student t test, and $P < .05$ was considered statistically significant.

Results

PCFT is essential for normal growth and survival

We generated *PCFT*-deficient mice by targeted disruption of the first 3 exons of the murine homolog of the *PCFT* gene (GenBank accession no. NM_026740) by homologous recombination in ESCs,[20] followed by germline transmission of the mutant gene into chimeric, *PCFT*$^{+/-}$, and *PCFT*$^{-/-}$ mice (Figure 1A). Southern hybridization analysis demonstrated the targeted mutation in ESCs (Figure 1B). *PCFT* transcripts were detected by reverse-transcribed PCR in all tissues of WT (*PCFT*$^{+/+}$) mice, except for adipose tissue and total bone tissue including BM (Figure 1C).

Mating of *PCFT*$^{+/-}$ mice generated pups of the 3 possible genotypes with ratios that fit well within normal Mendelian frequencies. However, *PCFT*$^{-/-}$ mice failed to thrive (body weight 21 ± 4 g, *PCFT*$^{+/+}$, n = 8 vs 15 ± 2 g, *PCFT*$^{-/-}$, n = 8, at 6 weeks of age, $P = .004$), and more than 90% of *PCFT* $^{-/-}$ mice died by 10 to 12 weeks of age. Growth rate and survival of *PCFT*$^{+/-}$ mice were normal; therefore, they were not routinely included in additional characterization studies.

A

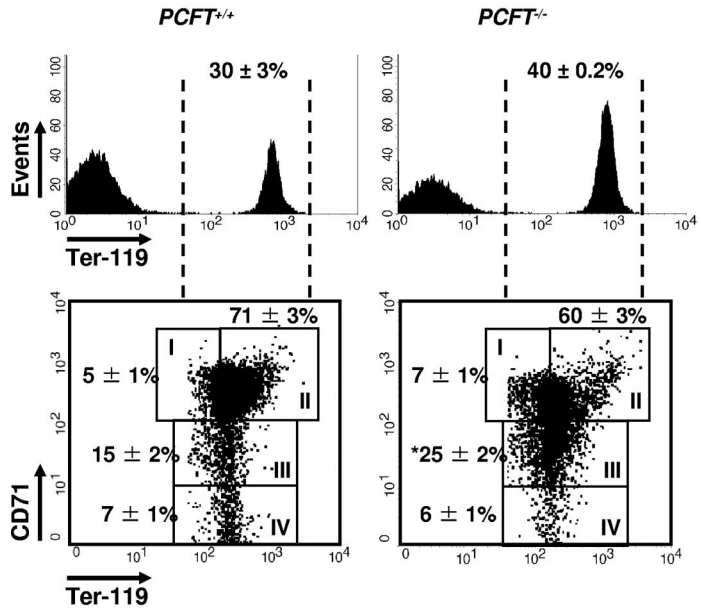

B

Bone Marrow

	(-/-)	(+/+)	p =
Cellularity (10^6/g)	1.6±0.1	2.0±0.1	0.023
% of positive cells. Gate : all viable cells			
Ter119+	40.2±2.2	29.6±2.7	0.006
CD71+	53.3±1.6	37.9±2.0	0.000
% of positive cells. Gate: Ter119+ cells			
$Ter119^{low}CD71^{high}$	6.5±0.8	4.8±1.0	0.179
$Ter119^{high}CD71^{high}$	59.8±2.5	71±2.7	0.007
$Ter119^{high}CD71^{med}$	25.1±2.0	15.3±2.4	0.005
$Ter119^{high}CD71^{low}$	5.9±0.6	7.4±0.5	0.078
Annexin V+ $Ter119^{high}CD71^{med}$	22±1.4	16.5±0.7	0.002

Spleen

	(-/-)	(+/+)	p =
Cellularity (10^6/g)	5.9±1.0	4.9±0.4	0.394
% of positive cells. Gate : all viable cells			
Ter119+	35.8±4.8	21.9±4.3	0.055
CD71+	38.3±4.6	22.2±4.2	0.023
% of positive cells. Gate: Ter119+ cells			
$Ter119^{low}CD71^{high}$	3.7±0.6	2.9±0.6	0.397
$Ter119^{high}CD71^{high}$	66.7±1.8	50.8±9.0	0.128
$Ter119^{high}CD71^{med}$	14.9±1.0	8.1±1.0	0.0002
$Ter119^{high}CD71^{low}$	12.5±1.5	35.7±8.3	0.023
Annexin V+ $Ter119^{high}CD71^{med}$	37.5±6.1	15.1±2.8	0.060

Figure 4. Erythroid differentiation is blocked at the late erythroblast stage in *PCFT*$^{-/-}$ mice. (A) BM cells of the indicated mice were analyzed by FACS for expression of the designated differentiation markers. Dashed vertical lines in the top histograms indicate the Ter119$^+$ cells analyzed in the bottom density plots. Rectangular gates represent proerythroblasts (I), early basophilic precursors (II), late basophilic and chromatophilic erythroblasts (III), and orthochromatophilic eryhthroblasts and reticulocytes (IV). Fraction of cells in the different maturation stages are indicated close to the respective gates (mean ± SEM; n = 10 mice each cohort). BM and splenic cellularity and the percentages of erythroid progenitor subsets in the BM and spleen, including the percentages of annexin V$^+$ intermediate erythroblasts, are summarized in panel B (mean ± SEM; n = 10 mice each cohort). Data are from one of 2 independent experiments showing similar results. *$P < .05$ compared with WTs.

Blood profile of *PCFT*$^{-/-}$ mice demonstrates pancytopenia and ineffective erythropoiesis

Hematologic analysis of the peripheral blood of *PCFT*$^{-/-}$ mice revealed decreased cellularity in all leukocyte populations as well as erythrocytes and platelets (Figure 2A). RBC parameters in the mutant mice were consistent with a diagnosis of macrocytic normochromic anemia, showing lower RBC counts and decreased HCT and hemoglobin concentration compared with WT controls, but having normal values for mean corpuscular hemoglobin concentration. In addition, increased distribution width of RBC indicated anisocytosis, which was accompanied by an increase in the mean corpuscular volume to the level of macrocytosis (mean corpuscular volume > 58 fL) in the majority of *PCFT*-deficient mice. Significant heterogeneity of RBC size in *PCFT*$^{-/-}$ mice, which leads to greater distribution width of RBC values, and anisocytosis, was observed in the *PCFT*$^{-/-}$ blood smears (not shown), which are indicative of active erythropoiesis leading to release of fully hemoglobinized macrocytes. Flow cytometric analysis revealed a significantly decreased response of erythropoietic tissues to anemia in *PCFT*$^{-/-}$ mice. Release of reticulocytes, expressed as a RPI, was consistently lower in *PCFT*$^{-/-}$ than WT controls (Figure 2B). The blood of *PCFT*$^{-/-}$ mice had elevated serum EPO and sCD71 concentrations (Figure 2D). The latter parameters are all indicators of ineffective erythropoiesis, a characteristic feature of folate deficiency anemia. As a probable compensatory response to severe thrombocytopenia, the serum concentration of thrombopoietin was also markedly elevated in *PCFT*$^{-/-}$ mice compared with WT animals (Figure 2D), along with increased mean platelet volume and size (Figure 2A and Figure 2C, respectively). The absolute number of newly formed rtPLTs in *PCFT*$^{-/-}$ mice was lower than that in WT controls (Figure 2C); however, the difference did not reach statistical significance because of an increase (data not shown) in the relative percentage of immature platelets with elevated mean platelet volume among the otherwise reduced total platelet population in *PCFT*$^{-/-}$ mice (Figure 2A). Pale skin and bloody stools noted in *PCFT*$^{-/-}$ mice along with pale livers and cerebral hemorrhages observed during necropsy (Figure 3D) were consistent with severe anemia and thrombocytopenia. Finally, the *PCFT*$^{-/-}$ blood smears showed multilobed polymorphonuclear neutrophils, which are characteristically observed in patients with folate deficiency anemia (Figure 3C).

Absence of PCFT leads to impaired erythropoiesis in the BM and spleen

The hematologic profile of *PCFT*-deficient mice closely resembled that of human folate deficiency anemia. This observation prompted

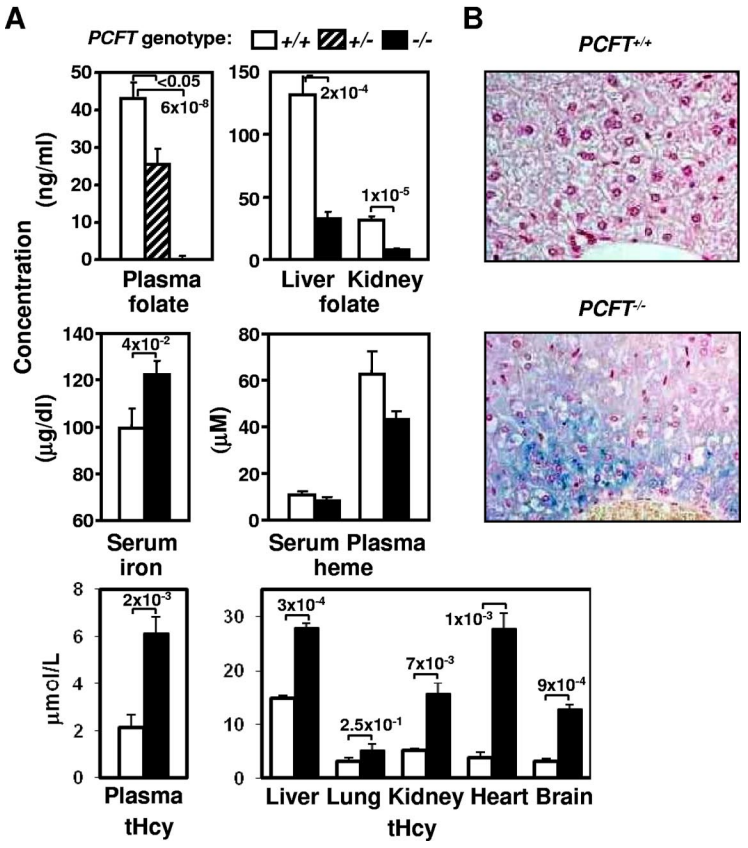

Figure 5. Absence of PCFT decreases systemic folate content and leads to iron and homocysteine buildup. (A) Concentration of folate, iron, heme, and tHcy in the indicated tissues was determined in 4- to 6-week-old mice of indicated genotype. Data are presented as in Figure 2; n = 12 mice in each cohort. (B) Gomori iron staining of liver sections (original magnification 40×/0.75 NA dry objective). Iron is detected in periportal hepatocytes of *PCFT*$^{-/-}$ mice mainly as fine cytoplasmic stippling and rarely as cytoplasmic granules on a diffuse light blue cytoplasmic background. Iron is not detected by Gomori staining in liver sections from WT animals.

us to characterize maturation and survival of RBC progenitors in *PCFT*$^{-/-}$ BM and spleen. Histopathologic examination revealed signs of marked erythroid cell hyperproliferation in the BM and spleens of *PCFT*$^{-/-}$ mice, leading to accumulation and overrepresentation of proerythroblasts and large basophilic erythroblasts (Figure 3A-B). However, both the reticular chromatin pattern and nucleocytoplasmic dissociation typically observed in human megaloblasts were infrequent findings in the *PCFT*$^{-/-}$ BM and splenic erythroblasts. The *PCFT*$^{-/-}$ BM also harbored less mature megakaryocytes with abnormal morphology. These findings are all consistent with a histopathologic profile observed in patients with folate deficiency anemia.

To delineate the erythroid maturational stages affected by the *PCFT* mutation, we performed phenotypic characterization of BM (Figure 4) and splenic (Figure 4B) subpopulations by FACS analysis using markers for erythroid cell differentiation and apoptosis. Differential expression of Ter119 and CD71 characterizes erythroid maturation, proceeding from proerythroblasts (Ter119^{low}CD71^{high} cells) and early basophilic precursors (Ter119^{high}CD71^{high}), through basophilic and chromatophilic erythroblasts (Ter119^{high}CD71^{med} intermediate erythroblasts), to orthochromatophilic erythroblasts and reticulocytes (Ter119^{high}CD71^{low} cells).[21] In *PCFT*-deficient mice, this maturational process appeared to be blocked at the intermediate erythroblast stage because the mutant BM showed accumulation of Ter119^{high}CD71^{med} intermediate erythroblasts compared with WT BM. Moreover, the proportion of annexin V-positive apoptotic cells was significantly higher in the intermediate erythroblast population of *PCFT*$^{-/-}$ BM than in the WT BM (22% ± 1.4% vs 16% ± 0.7%; $P = .006$), indicating that erythroid differentiation in the mutant BM was impaired as a result of decreased survival of erythroblasts at the later stage of erythroid maturation. Ineffective erythropoiesis and elevated EPO levels in *PCFT*$^{-/-}$ mice also led to the rapid expansion of stress erythroid progenitors in the spleen, the primary site of extramedullary erythropoiesis in mice (Figure 4B). However, the expansion of TER119^{+} erythroid progenitors and accumulation of Ter119^{high}CD71^{med} intermediate erythroblasts in the spleen of *PCFT*$^{-/-}$ mice was accompanied by elevated apoptosis in the intermediate erythroblast subset of *PCFT*$^{-/-}$ splenocytes, resulting in only a modest increase in splenic cellularity (Figure 4B).

PCFT is indispensable for normal intestinal uptake and tissue accumulation of folate

Previous studies have described PCFT as a low pH-dependent folate transporter contributing to dietary folate absorption in humans.[6-8] The presence of hematologic abnormalities in PCFT-deficient mice was also consistent with systemic folate deficiency; therefore, we measured folate concentrations in the peripheral blood and tissues that are known to have high folate content. Plasma, liver, and kidney folate concentrations were all significantly decreased in *PCFT*$^{-/-}$ and *PCFT*$^{+/-}$ mice compared with WT littermates (Figure 5A). In contrast, serum concentration of total iron was increased in the mutant mice, which is in agreement with previous reports of elevated systemic iron levels observed during folate deficiency.[22] Liver sections of the mutant mice also showed increased iron accumulation (Figure 5B). On the other hand, *PCFT*$^{-/-}$ mice registered normal serum and plasma heme concentration (Figure 5A), suggesting that deficiency in heme is not a contributor to the anemia in *PCFT*$^{-/-}$ mice. Folate depletion is also associated with hyperhomocysteinemia; therefore, *PCFT*$^{-/-}$ mice were expected to have elevated

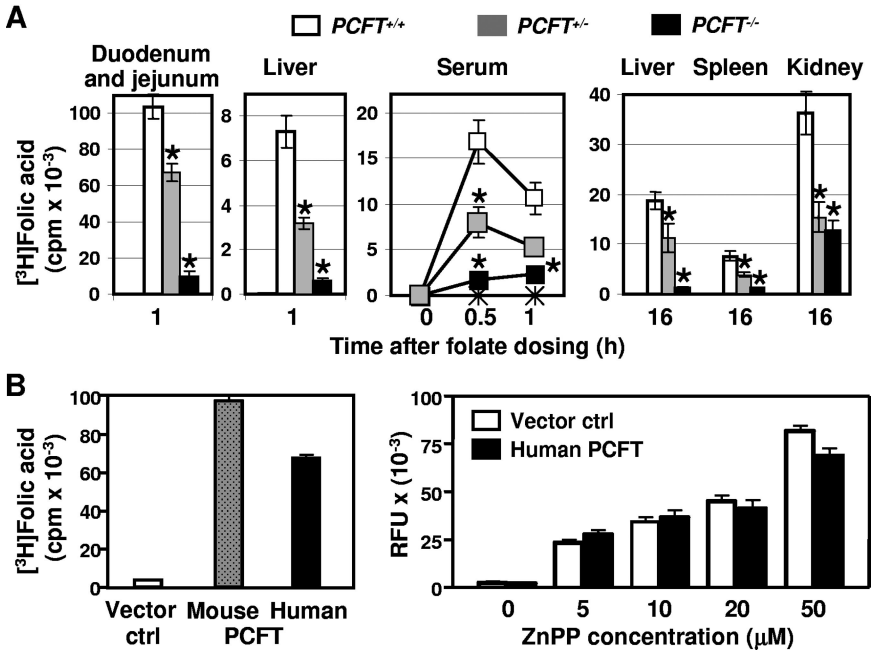

Figure 6. PCFT is essential for intestinal folate uptake and tissue accumulation. (A) In vivo uptake of tritiated folic acid to the indicated tissues was measured at the time points shown. (B) Uptake of folate and zinc protoporphyrin (ZnPP) by HEK293 cells transiently transfected with vector only or with mouse or human *PCFT*, as indicated, was measured. Data are presented as in Figure 2. $^*P < .05$.

tissue content of homocysteine. Observations confirmed increased tHcy concentration in plasma, brain, heart, lungs, liver, and kidney of $PCFT^{-/-}$ mice (Figure 5A).

The main source of folate in uptake is through intestinal absorption. To investigate the role of PCFT in the intestinal transport of folate in vivo, we analyzed the kinetics of folate uptake into various tissues in WT and *PCFT*-deficient mice after oral gavage administration of radioactively labeled folic acid. As shown in Figure 6A, both homozygous and heterozygous deletion of the PCFT gene led to a dramatic decrease in duodenum-jejunum folate one hour after the oral folate, supporting the essential role of PCFT in the intestinal uptake of folate. In agreement with the deficient intestinal uptake, systemic accumulation of folate in serum, liver, kidney, and spleen was dramatically lower in $PCFT^{-/-}$ and $PCFT^{-/+}$ mice compared with that in WT mice.

To further confirm the function of PCFT as a folate transporter, we measured folate uptake in HEK293 cells transiently transfected with either human or mouse PCFT. PCFT of either species facilitated robust cellular uptake of radioactively labeled folate, whereas cells transfected with vector alone showed no significant uptake of folate (Figure 6B). Of note, uptake of zinc protoporphyrin, a measure of heme transport activity, was not affected by expression of the human PCFT in the same cell line.

Folates rescue $PCFT^{-/-}$ mice

To further investigate the role of PCFT in the intestinal transport of folates in vivo, we tested various folate supplementation strategies to demonstrate the biologic function of PCFT. $PCFT^{-/-}$ mice develop folate deficiency anemia and die prematurely because of these conditions, so rescue strategies were developed to increase the length of survival of null pups resulting from PCFT's function as a folate or heme transporter. Subcutaneous injections of 5-formyltetrahydrofolate (folinic acid), 5-MTHF, or folic acid promoted survival in $PCFT^{-/-}$ mice and significantly improved RBC and platelet parameters, including RBC and platelet counts, HCT, and hemoglobin concentration (Figure 7). The results confirmed that folates are the essential nutrients deficient in the $PCFT^{-/-}$ mice, and their replacement via the parenteral route is sufficient to rescue $PCFT^{-/-}$ mice from premature death. Oral supplementation with 5-MTHF at 10 to 40 mg/kg per day also rescued $PCFT^{-/-}$ mice from anemia and thrombocytopenia, indicating sustained transport of 5-MTHF across the gastrointestinal epithelia in the absence of PCFT. In contrast, daily oral supplementation with folic acid at a therapeutic dose (0.1 mg/kg) failed to rescue $PCFT^{-/-}$ mice from anemia and premature death. However, when $PCFT^{-/-}$ mice were treated orally with high doses of folic acid (2 mg/kg), folic acid therapy significantly increased survival and improved RBC and platelet parameters, suggesting the involvement of alternative transport systems in the intestinal uptake of folic acid given at supraphysiologic concentrations. No increases in survival rates were observed in $PCFT^{-/-}$ mice supplemented with oral betaine, folinic acid, $FeSO_4$, or hemin injections (data not shown).

Discussion

The PCFT knockout model presented here provides in vivo evidence for a pivotal and nonredundant role played by PCFT in intestinal folate absorption and erythropoiesis. Inactivation of the PCFT gene resulted in a marked decrease of folate uptake in the duodenum-jejunum, leading to folate deficiency. The phenotype of *PCFT*-mutant mice presented in this report largely recapitulated the hematologic phenotype of dietary folate deficiency in mice and closely resembles the type of anemia reported in folate-deficient humans.[22,23] In mice, the key features of folate deficiency are growth retardation, anemia associated with a marked, progressive macrocytosis, and pancytopenia[22,24] accompanied by ineffective hematopoiesis in the BM and spleen.[22,25] In humans, the disease of folate malabsorption is characterized as macrocytic/megaloblastic anemia because of the accumulation of large immature erythroid progenitors, which undergo apoptosis before complete maturation resulting from impaired DNA synthesis.[2] Likewise, in the absence of the PCFT-mediated intestinal folate transport, mice developed systemic folate deficiency and severe macrocytic normochromic anemia with normal corpuscular hemoglobin and elevated corpuscular volume. $PCFT^{-/-}$ BM showed accumulation of immature

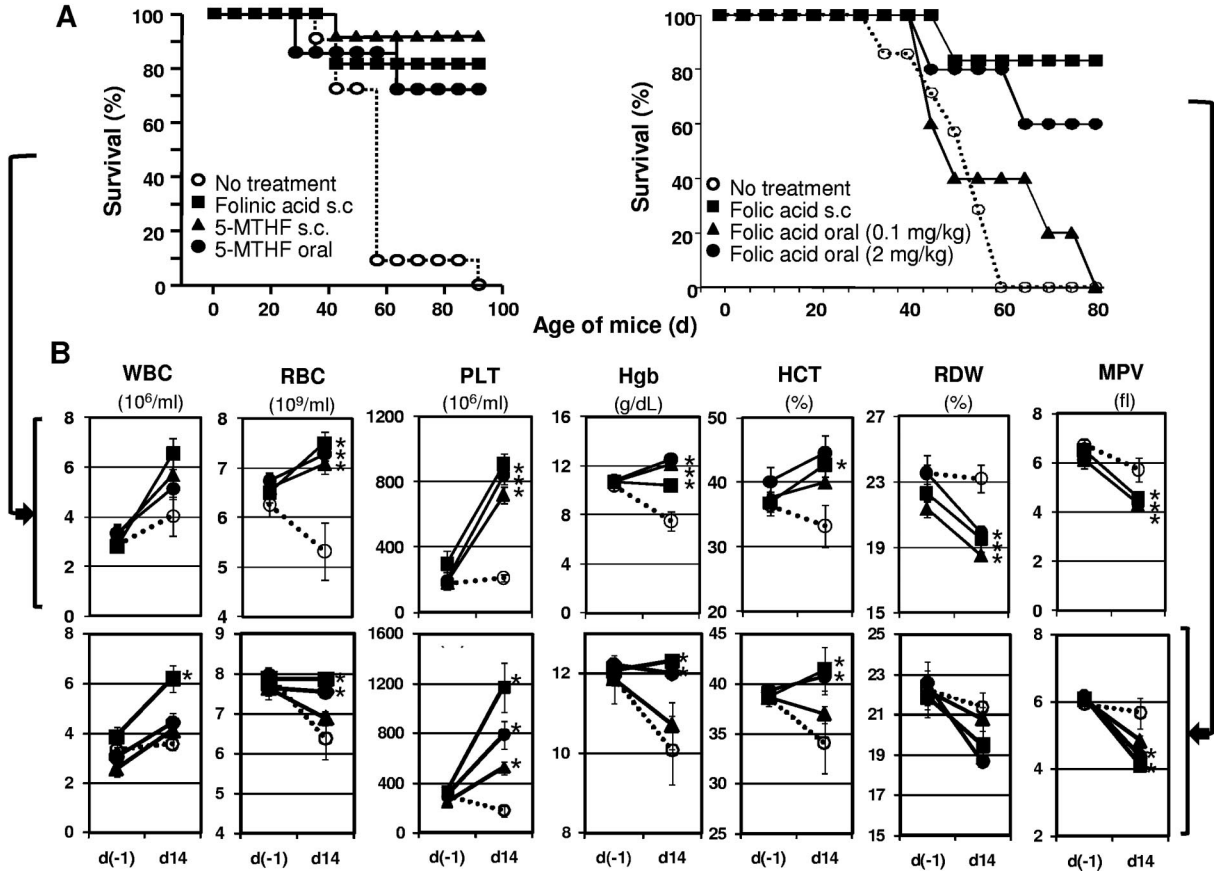

Figure 7. Folate supplementation rescues *PCFT*$^{-/-}$ mice. Survival curves (A) and hematologic profile (B) are presented for mice treated with the indicated supplements (n = 6-12 mice per cohort). s.c. indicates subcutaneous injection; d(-1), day −1 of folate supplementation; and d14, day 14 of folate supplementation. *$P < .05$.

intermediate erythroblasts, which failed to differentiate further and showed increased rate of apoptosis similarly to proerythroblasts isolated from mice fed an amino acid-based, folate-free diet.[25] Marked expansion of erythroid *PCFT*$^{-/-}$ precursors and elevated apoptosis of intermediate *PCFT*$^{-/-}$ erythroblasts were also evident in the spleen, the primary site of extramedullary erythropoiesis in mice. Consistent with ineffective erythropoiesis and enhanced intramedullary destruction of erythroblasts, we observed an increase in soluble transferrin receptor serum levels in *PCFT*$^{-/-}$ mice. Serum soluble transferrin receptor, a truncated monomer of cell surface-expressed transferrin receptor, is primarily released from erythroblasts, and its serum level reflects the erythropoietic activity of BM and spleen.[26,27] We also observed multilobed polymorphonuclear neutrophils in the *PCFT*$^{-/-}$ blood smears and giant metamyelocytes in the *PCFT*$^{-/-}$ BM, consistent with abnormal myelopoiesis often observed in patients with folate deficiency-induced anemia. Internal bleeding in the cerebral vasculature and bloody stools were also noted in *PCFT*$^{-/-}$ mice, which too is often associated with folate deficiency-induced anemia. Therefore, PCFT deficiency in mice presents a bona fide model of hereditary folate malabsorption syndrome and folate deficiency anemia, recapitulating all the key indicators of the disease. It is also noteworthy that deletion of a single allele of *PCFT* leads to haploinsufficiency and phenotypic abnormalities in the intestinal transport of folate in vivo, resulting in a systemic folate deficiency. These findings are in agreement with the previous studies in humans diagnosed with hereditary folate malabsorption, indicating that heterozygosity for loss-of-function *PCFT* mutations results in a clinically significant decrease in folate absorption.[6,28-30]

It was noted that the majority of *PCFT*-mutant mice appeared normal before they were weaned. We therefore hypothesized that forms of folate in the dam's milk were able to maintain early development, but the synthetic folic acid in adult chow was unable to cross the intestinal epithelia. The folate form found in milk tends to be 5-MTHF, which will dissociate with FOLR1 during gastric passage, but would be expected to bind RFC-1 with relatively high affinity (~ 2μM), compared with folic acid (~ 200μM) in the lower intestinal tract.[31-33] We therefore tested whether 5-MTHF or folinic acid (40 mg/kg) could rescue *PCFT*-mutant mice from early death. Oral supplementation with 5-MTHF rescued the majority of *PCFT*-mutant mice from early death, anemia, and thrombocytopenia, as did injections with folic acid, 5-MTHF, or folinic acid. Increased survival and improved hematopoietic competency in *PCFT*$^{-/-}$ mice treated with parenteral folic acid are consistent with the biotransformation of folic acid and sufficient uptake of reduced folic acid derivatives in tissues. Although oral supplementation with pharmacologic doses of folic acid failed to rescue *PCFT*$^{-/-}$ mice from premature death and impaired hematopoiesis, except for a slight increase in platelet counts, *PCFT*$^{-/-}$ mice supplemented orally with high doses of folic acid displayed a significant increase in survival accompanied by improved RBC and platelet parameters. These findings confirm earlier studies indicating that relatively low folate levels are sufficient to correct hematopoietic abnormalities in patients with hereditary folate malabsorption, whereas

repeated administration of high doses of folic acid is required to increase folate levels in the cerebrospinal fluid and compensate for impaired folate transport into the brain.[30,34] Direct analysis of the cerebrospinal fluid/serum ratio in *PCFT*-mutant mice will be required to validate this hypothesis and is currently underway.

Finally, after maturity, supplementation was reduced to weekly doses, and *PCFT*-mutant mice were noted to live in excess of 300 days, but all *PCFT*-mutant mice redeveloped folate deficiency anemia 4 to 6 weeks after experimental supplementation was discontinued (R.M.C. and R.H.F., unpublished data, April 6, 2010).

Without proper supplementation, the *PCFT*-mutant mice displayed several additional abnormal blood parameters that are all typical diagnostic biomarkers for human megaloblastic anemia and reflect the response of BM to anemia and inefficient hematopoietic cell maturation. These included: (1) reduced release of reticulocytes from the BM and spleen resulting from a block in erythroid cell maturation, (2) thrombocytopenia accompanied by abnormal thrombocytopoiesis and underproduction of platelets, (3) increased serum thrombopoietin concentration as a response to thrombocytopenia, and (4) elevated EPO, sCD71, and iron concentration in the serum resulting from the increased but inefficient erythropoietic activity. Greater iron concentration was also observed in animals fed with folate-deficient diet[22] and could be explained by diminished use of iron for synthesis of hemoglobin in the deficient animals. The elevated iron content and normal heme levels rule out both iron and heme deficiency as a probable cause of anemia in the $PCFT^{-/-}$ mice. Even though PCFT has been originally described as a heme carrier protein,[14] we, like others,[6,8] could not detect PCFT-related heme transport in vitro, and the normal heme content of blood in the absence of PCFT indicates that this transporter does not play a significant role in heme uptake in vivo. Furthermore, our folate supplementation studies indicate that the heme transport function of PCFT is not essential for normal erythropoiesis as oral supplementation with 5-MTHF in *PCFT*-mutant mice resulted in the complete rescue from anemia and normalized the length of survival of the nullizygous pups. These findings underline the critical role of PCFT in folate uptake both in vitro and in vivo and provide in vivo evidence for a redundant function of PCFT in heme uptake and metabolism.

Systemic folate deficiency in patients with hereditary folate malabsorption is accompanied by a severe progressive neurologic disorder and intracranial calcifications.[30] However, no evidence of calcification was identified in any sections of $PCFT^{-/-}$ brain tissue by hematoxylin and eosin and von Kossa staining. It is probable that calcification appears in $PCFT^{-/-}$ animals in an age-dependent manner and premature death precludes detection of intracranial calcifications by standard histologic techniques. Finally, our findings suggest that severe thrombocytopenia may lead to subdural or subarachnoid hemorrhages observed in some $PCFT^{-/-}$ mice macroscopically. However, histologic examination failed to detect deep intracerebral hemorrhages in $PCFT^{-/-}$ brain sections. Hemorrhages associated with thrombocytopenia may develop in patients with megaloblastic anemia,[35] and this clinical manifestation of folate deficiency is recapitulated in the *PCFT* knockout model.

Existing genetic models of folate transport and deficient erythropoiesis only partially replicate common clinical manifestations of human megaloblastic anemia. Targeted disruption of the other folate transporters, *RFC1* and *FOLR1*, results in embryonic lethality in mice.[5,10] Inactivation of the methionine synthase gene (*MS*), a B12-dependent enzyme required for demethylation of 5-MTHF to tetrahydrofolate, would be expected to produce a functional folate deficiency by trapping folate as 5-MTHF. However, *MS* deletion leads to embryonic lethality because of the methyl trap, whereas heterozygous $MS^{+/-}$ mice fail to develop anemia.[36] Megaloblastic erythroid development was described in a mouse model of thiamine-responsive megaloblastic anemia syndrome.[37] Erythroid cells from mice deficient for the high-affinity thiamine transporter, Slc19a2, demonstrated altered thiamine uptake. Accordingly, $Slc19a2^{-/-}$ mice showed some distinctive features of megaloblastic anemia with erythroid hyperplasia in the BM, ineffective erythropoiesis with a dys-synchrony of nuclear and cytoplasmic maturation, increased lobulation of megakaryocytes, and accumulation of giant metamyelocytes.[37] Although these changes affecting erythroid, myeloid, and megakaryocyte lineages are reminiscent of megaloblastic erythroid maturation, it remains undocumented whether $Slc19a2^{-/-}$ mice develop pancytopenia as a result of dysregulated erythropoiesis, thrombopoiesis, and myelopoiesis in the BM, and whether the ineffective erythropoiesis in $Slc19a2^{-/-}$ mice stems from increased apoptosis of late erythroblasts, which is the hallmark of megaloblastic erythropoiesis. Moreover, the phenotypic expression of *Slc19a2* homozygosity in the erythroid lineage was documented in the absence of systemic folate deficiency and only in $Slc19a2^{-/-}$ mice challenged with thiamine-deficient diet, thus limiting the relevance of the model to folate deficiency-dependent megaloblastic erythropoiesis. Finally, Fleming et al[38] found no evidence of megaloblastosis in the BM of $Slc19a2^{-/-}$ mice.

In conclusion, the PCFT-deficient mouse line is the most accurate animal model that closely captures the spectrum of pathology typical of human hereditary folate malabsorption syndrome and human folate deficiency anemia. The primary cause of the disease is a disruption of PCFT-mediated intestinal folate uptake, yet the results presented here do not rule out the possibility that PCFT may control folate uptake in other tissues as well. Future studies using *PCFT* KO mice will help determine the physiologic function of this transporter in more detail and facilitate identification of factors involved in the pathologic mechanisms leading to ineffective hematopoiesis.

Acknowledgments

The authors thank the phenotypic analysis groups at Lexicon Pharmaceuticals Inc, for carrying out the comprehensive clinical diagnostic tests on the *PCFT* mutant mouse line, and C.A. Turner for critical reading of the manuscript.

This work was supported by the Albert and Margaret M. Alkek Foundation and the Texas A&M Institute for Genomic Medicine (R.M.C., R.H.F.).

Authorship

Contribution: K.V.S. designed experiments, analyzed data, and wrote the manuscript with extensive contributions from R.M.C., K.A.P., Q.L., R.R., W.C.C., and P.V.; T.O. and R.H.F. edited the manuscript and provided conceptual advice; T.O., R.H.F., K.V.S., and R.M.C. supervised the project; and W.S., W.C.C., C.L., and L.D. performed the experiments.

Conflict-of-interest disclosure: K.V.S., W.S., W.C.C., C.L., L.D., K.A.P., R.R., P.V., Q.L., and T.O. are or have been employees of, and received stock options from, Lexicon Pharmaceuticals Inc. The remaining authors declare no competing financial interests.

The current affiliation of R.M.C. and R.H.F. is Department of Nutritional Sciences, University of Texas at Austin, Austin, TX.

Correspondence: Konstantin V. Salojin, Lexicon Pharmaceuticals Inc, 8800 Technology Forest Pl, The Woodlands, TX 77381; e-mail: ksalojin@lexpharma.com.

References

1. Hentze MW, Muckenthaler MU, Andrews NC. Balancing acts: molecular control of mammalian iron metabolism. *Cell.* 2004;117(3):285-297.
2. Koury MJ, Ponka P. New insights into erythropoiesis: the roles of folate, vitamin B12, and iron. *Annu Rev Nutr.* 2004;24:105-131.
3. Williams FM, Murray RC, Underhill TM, Flintoff WF. Isolation of a hamster cDNA clone coding for a function involved in methotrexate uptake. *J Biol Chem.* 1994;269(8):5810-5816.
4. Tolner B, Roy K, Sirotnak FM. Organization, structure and alternate splicing of the murine RFC-1 gene encoding a folate transporter. *Gene.* 1997;189(1):1-7.
5. Piedrahita JA, Oetama B, Bennett GD, et al. Mice lacking the folic acid-binding protein Folbp1 are defective in early embryonic development. *Nat Genet.* 1999;23(2):228-232.
6. Qiu A, Jansen M, Sakaris A, et al. Identification of an intestinal folate transporter and the molecular basis for hereditary folate malabsorption. *Cell.* 2006;127(5):917-928.
7. Zhao R, Qiu A, Tsai E, Jansen M, Akabas MH, Goldman ID. The proton-coupled folate transporter: impact on pemetrexed transport and on antifolates activities compared with the reduced folate carrier. *Mol Pharmacol.* 2008;74(3):854-862.
8. Nakai Y, Inoue K, Abe N, et al. Functional characterization of human proton-coupled folate transporter/heme carrier protein 1 heterologously expressed in mammalian cells as a folate transporter. *J Pharmacol Exp Ther.* 2007;322(2):469-476.
9. Chiao JH, Roy K, Tolner B, Yang CH, Sirotnak FM. RFC-1 gene expression regulates folate absorption in mouse small intestine. *J Biol Chem.* 1997;272(17):11165-11170.
10. Zhao R, Russell RG, Wang Y, et al. Rescue of embryonic lethality in reduced folate carrier-deficient mice by maternal folic acid supplementation reveals early neonatal failure of hematopoietic organs. *J Biol Chem.* 2001;276(13):10224-10228.
11. Gelineau-van Waes J, Heller S, Bauer LK, et al. Embryonic development in the reduced folate carrier knockout mouse is modulated by maternal folate supplementation. *Birth Defects Res A Clin Mol Teratol.* 2008;82(7):494-507.
12. Birn H, Spiegelstein O, Christensen EI, Finnell RH. Renal tubular reabsorption of folate mediated by folate binding protein 1. *J Am Soc Nephrol.* 2005;16(3):608-615.
13. Salbaum JM, Finnell RH, Kappen C. Regulation of folate receptor 1 gene expression in the visceral endoderm. *Birth Defects Res A Clin Mol Teratol.* 2009;85(4):303-313.
14. Shayeghi M, Latunde-Dada GO, Oakhill JS, et al. Identification of an intestinal heme transporter. *Cell.* 2005;122(5):789-801.
15. Zhao R, Min SH, Wang Y, Campanella E, Low PS, Goldman ID. A role for the proton-coupled folate transporter (PCFT-SLC46A1) in folate receptor-mediated endocytosis. *J Biol Chem.* 2009;284(7):4267-4274.
16. Cabrera RM, Shaw GM, Ballard JL, et al. Autoantibodies to folate receptor during pregnancy and neural tube defect risk. *J Reprod Immunol.* 2008;79(1):85-92.
17. Jacobsen DW, Gatautis VJ, Green R. Determination of plasma homocysteine by high-performance liquid chromatography with fluorescence detection. *Anal Biochem.* 1989;178(1):208-214.
18. Gupta S, Kuhnisch J, Mustafa A, et al. Mouse models of cystathionine beta-synthase deficiency reveal significant threshold effects of hyperhomocysteinemia. *FASEB J.* 2009;23(3):883-893.
19. Eisenga BH, Collins TD, McMartin KE. Incorporation of 3H-label from folic acid is tissue-dependent in folate-deficient rats. *J Nutr.* 1992;122(4):977-985.
20. Wattler S, Kelly M, Nehls M. Construction of gene targeting vectors from lambda KOS genomic libraries. *Biotechniques.* 1999;26(6):1150-1156.
21. Socolovsky M, Nam H, Fleming MD, Haase VH, Brugnara C, Lodish HF. Ineffective erythropoiesis in Stat5a(−/−)5b(−/−) mice due to decreased survival of early erythroblasts. *Blood.* 2001;98(12):3261-3273.
22. Bills ND, Koury MJ, Clifford AJ, Dessypris EN. Ineffective hematopoiesis in folate-deficient mice. *Blood.* 1992;79(9):2273-2280.
23. Celada A, Rudolf H, Donath A. Effect of experimental chronic alcohol ingestion and folic acid deficiency on iron absorption. *Blood.* 1979;54(4):906-915.
24. MacGregor JT, Schlegel R, Wehr CM, Alperin P, Ames BN. Cytogenetic damage induced by folate deficiency in mice is enhanced by caffeine. *Proc Natl Acad Sci U S A.* 1990;87(24):9962-9965.
25. Koury MJ, Horne DW, Brown ZA, et al. Apoptosis of late-stage erythroblasts in megaloblastic anemia: association with DNA damage and macrocyte production. *Blood.* 1997;89(12):4617-4623.
26. Beguin Y, Loo M, R'Zik S, et al. Quantitative assessment of erythropoiesis in haemodialysis patients demonstrates gradual expansion of erythroblasts during constant treatment with recombinant human erythropoietin. *Br J Haematol.* 1995;89(1):17-23.
27. Beguin Y. Soluble transferrin receptor for the evaluation of erythropoiesis and iron status. *Clin Chim Acta.* 2003;329(1):9-22.
28. Zittoun J. Congenital errors of folate metabolism. *Baillieres Clin Haematol.* 1995;8(3):603-616.
29. Zhao R, Min SH, Qiu A, et al. The spectrum of mutations in the PCFT gene, coding for an intestinal folate transporter, that are the basis for hereditary folate malabsorption. *Blood.* 2007;110(4):1147-1152.
30. Geller J, Kronn D, Jayabose S, Sandoval C. Hereditary folate malabsorption: family report and review of the literature. *Medicine (Baltimore).* 2002;81(1):51-68.
31. Verwei M, Arkbage K, Mocking H, Havenaar R, Groten J. The binding of folic acid and 5-methyltetrahydrofolate to folate-binding proteins during gastric passage differs in a dynamic in vitro gastrointestinal model. *J Nutr.* 2004;134(1):31-37.
32. Wang Y, Zhao R, Russell RG, Goldman ID. Localization of the murine reduced folate carrier as assessed by immunohistochemical analysis. *Biochim Biophys Acta.* 2001;1513(1):49-54.
33. Goldman ID. The characteristics of the membrane transport of amethopterin and the naturally occurring folates. *Ann N Y Acad Sci.* 1971;186:400-422.
34. Corbeel L, Van den Berghe G, Jaeken J, Van Tornout J, Eeckels R. Congenital folate malabsorption. *Eur J Pediatr.* 1985;143(4):284-290.
35. Smith MD, Smith DA, Fletcher M. Haemorrhage associated with thrombocytopenia in megaloblastic anaemia. *Br Med J.* 1962;1(5283):982-985.
36. Swanson DA, Liu ML, Baker PJ, et al. Targeted disruption of the methionine synthase gene in mice. *Mol Cell Biol.* 2001;21(4):1058-1065.
37. Oishi K, Hofmann S, Diaz GA, et al. Targeted disruption of Slc19a2, the gene encoding the high-affinity thiamin transporter Thtr-1, causes diabetes mellitus, sensorineural deafness and megaloblastosis in mice. *Hum Mol Genet.* 2002;11(23):2951-2960.
38. Fleming JC, Tartaglini E, Kawatsuji R, et al. Male infertility and thiamine-dependent erythroid hypoplasia in mice lacking thiamine transporter Slc19a2. *Mol Genet Metab.* 2003;80(1):234-241.